Atomic Resolution Study of Reversible Conversion Reaction in Metal Oxide Electrodes for Lithium-Ion Battery

Langli Luo,[†,§] Jinsong Wu,*,[†,§] Junming Xu,[†,‡] and Vinayak P. Dravid*,[†]

[†]Department of Materials Science and Engineering, NUANCE Center, Northwestern University, Evanston, Illinois 60208, United States and [‡]College of Electronic Information, Hangzhou Dianzi University, Hangzhou, China. [§]These authors (L.L. and J.W.) contributed equally to this work.

ABSTRACT Electrode materials based on conversion reactions with lithium ions have shown much higher energy density than those based on intercalation reactions. Here, nanocubes of a typical metal oxide (Co_3O_4) were grown on few-layer graphene, and their electrochemical lithiation and delithiation were investigated at atomic resolution by *in situ* transmission electron microscopy to reveal the mechanism of the reversible conversion reaction. During lithiation, a lithium-inserted Co_3O_4 phase and a phase consisting of nanosized Co—Li—O clusters are identified as the intermediate products prior to

the subsequent formation of Li_2O crystals. In delithiation, the reduced metal nanoparticles form a network and breakdown into even smaller clusters that act as catalysts to prompt reduction of Li_2O, and CoO nanoparticles are identified as the product of the deconversion reaction. Such direct real-space, real-time atomic-scale observations shed light on the phenomena and mechanisms in reaction-based electrochemical energy conversion and provide impetus for further development in electrochemical charge storage devices.
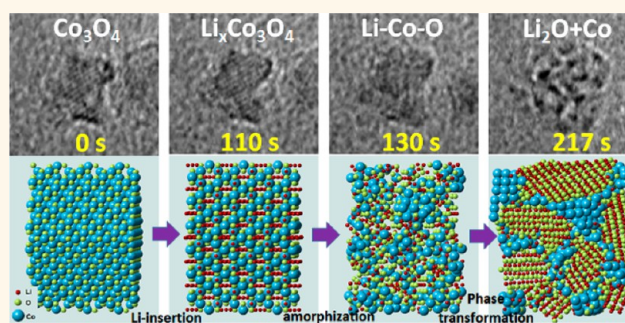
KEYWORDS: conversion/deconversion reaction · lithium-ion battery · *in situ* high-resolution electron microscopy · metal oxide electrode · electron diffraction

Intercalation and deintercalation reactions between lithium ions and electrode materials are commonly utilized in most commercial lithium-ion batteries to reversibly store and release chemical energy. Insertion materials such as graphite and $LiCoO_2$ host lithium ions in the lattice and incur small structural changes, thus such batteries have excellent cyclic performance. However, the lithium storage capacity is small due to the limited host sites in the intercalation materials; that is, 1 mol of $LiCoO_2$ (with a capacity of ~145 mAh g^{-1}) can host and extract no more than 0.5 mol of lithium. Alternatively, alloying and conversion reactions are found to represent other mechanisms for uptake and extraction of lithium and are able to sustain large lithium capacity.[1−3] Conversion reactions are observed for a series of metal oxides, fluorides, nitrides, phosphides, and hydrides where the metal salt is reacted with lithium to form fine metal particles embedded in lithium salt, sustaining large

capacity, for example, a theoretical capacity of 890 mAh g^{-1} for Co_3O_4.

For most of the metal oxides, the lithiation/conversion reaction $M_xO_y + 2yLi^+ + 2ye^- = xM_0 + yLi_2O$ is thermodynamically feasible and has a positive electromotive force.[4] Here, Li_2O has been identified as the product of lithiation. Li_2O is generally less active than Li_2O_2. Li_2O_2 is the product generally identified in a lithium—air battery by direct reaction of lithium with oxygen. The decomposition of Li_2O in the delithiation/deconversion reaction ($xM_0 + yLi_2O = M_xO_y + 2yLi^+ + 2ye^-$) involves cleavage of stable Li—O bonds. It remains unclear how the electrochemically inactive Li_2O can be reduced in the delithiation cycle to form lithium and metal oxide, as it has been shown that a simple mixture of metal nanoparticle and Li_2O is inactive[2] or has inferior and different electrochemical properties.[5−7] Overpotential, voltage hysteresis, extremely low initial Coulombic efficiency in the first cycle (typically 65−70%), and additional

reversible capacities shown beyond the theoretical capacity are intriguing phenomena associated with battery systems that are based on conversion/deconversion reactions. Recently, it has been shown that the reversible formation and decomposition of a secondary electrolyte interface phase, such as LiOH, Li_2O, and LiH, is a major contributor to this additional capacity.[8] Voltage hysteresis, referring to asymmetry of the voltage capacity profiles in the discharge/charge cycle, may be caused by a different reaction pathway of conversion and deconversion. Greater understanding of the reaction mechanism is clearly needed to understand, and thereby tailor, these phenomena.

In situ transmission electron microscopy (TEM) has been shown to be a uniquely helpful technique in revealing the underlying mechanism of lithium-ion batteries.[9−14] Here, we have investigated the lithiation (conversion) and delithiation (deconversion) processes at atomic resolution of uniform Co_3O_4 nanocubes (about 5 nm) anchored on a few-layer graphene synthesized by a simple hydrothermal method. In the first cycle, when lithium ions are diffused to Co_3O_4, the lithium ions inserted into Co_3O_4 crystalline lattice caused a small amount (∼14%) of volume expansion at the beginning of lithiation. The further intake of lithium ion leads to a collapse of the Co_3O_4 crystalline lattice, then formation of a phase consisting of Li−Co−O clusters and finally networks of Co nanoparticles reduced to a nominal size of <1 nm surrounded by Li_2O, as observed at atomic resolution by in situ high-resolution electron microscopy (HREM). The crystalline and microstructural evolutions of Co_3O_4 and graphene nanosheets were monitored by in situ low-dose nanobeam electron diffraction. In particular, we did not observe the signature of Li_2O_2, confirming that Li_2O is the major lithium oxide involved in the electrochemical cycles. In delithiation, when lithium ions are electrochemically extracted from the Co and Li_2O composite, the Co nanoparticles breakdown into even smaller clusters to react with the oxygen anion, leading to the decomposition of Li_2O and formation of CoO (instead of the original Co_3O_4) nanoparticles. This is one of the causes of the extremely low initial Coulombic efficiency. The direct observation of lithiation/delithiation along with the formation of Li_2O at atomic resolution has implications for the understanding of the conversion and deconversion reactions in a wide range of materials, as well as providing a combined in situ TEM technique to characterize essential and novel electrode materials for batteries.

RESULTS AND DISCUSSION

Lithiation (Conversion Reaction) with Insertion of a Lithium Ion. Figure 1A shows a scanning electron microscopy (SEM) image of the cobalt oxide nanocubes grown on few-layer graphene using a simple hydrothermal method. The phase was identified by selected area electron diffraction (SAED) (Figure 1B) as the spinel form of Co_3O_4 with a theoretical capacity of 890 mAh g^{-1}. The Co_3O_4 nanocubes have an average size of ∼5 nm, as shown in Figure 1C. The sample of Co_3O_4 nanocubes on graphene (Co_3O_4/graphene) was selected so that the synergetic effects of the few-layer graphene and Co_3O_4 in the lithiation and delithiation cycles could be studied. A half-cell miniature battery consisting of Co_3O_4/graphene, Li_2O electrolyte, and Li metal was assembled by using an in-house-modified Nanofactory electrical biasing holder for high-resolution in situ observations. The tested electrode materials (Co_3O_4/graphene) had no direct contact with the electrolyte and Li_2O/Li until they were inserted into a TEM, as shown in Figure 1D. Once they were connected and when a potential (normally −3 V) was applied, charging for the Co_3O_4/graphene composite occurred, corresponding to the bias-induced electrochemical lithiation and conversion reaction of Co_3O_4. As can be seen in the low-magnification TEM image (Figure 1E) and Supporting Information movie 1, the Co_3O_4 nanocubes have been decomposed, forming a uniform compound with much finer nanoparticles (as shown as black dots) in the matrix.

During lithiation, the phase evolutions in the electrochemical conversion reaction has been monitored by in situ SAED. We cannot identify Li_2O_2 in any diffraction patterns, suggesting its complete absence or minimal presence within constraints of our experimental setting. An intermediate stage with the formation of Co-rich Co−Li−O clusters is observed when the Co_3O_4 nanocubes disintegrated, while Li_2O crystals are not yet formed. The Co−Li−O clusters are gradually reduced to Co^0 clusters with further intake of lithium ions and formation of Li_2O nanocrystals. As seen in Supporting Information Figure 1A−D, the diffraction rings of the spinel Co_3O_4 structure gradually disappear as the reaction progresses (e.g., the {222} ring marked by a red arrowhead becomes gradually weaker and disappears at approximately 171 s in the present experiment). The diffused ring corresponding to the Co-rich clusters appeared at about 86 s. This is much earlier than the appearance of the diffraction rings of Li_2O at about 171 s, as shown in Supporting Information Figure 1B−F, in which the diffused diffraction ring is marked by yellow arrowheads and Li_2O rings by blue arrowheads.

The d-spacing in real space of the diffused ring ranges from 0.20 to 0.21 nm as measured from the pattern, comparable to 0.205 nm of the {111} spacing of body-centered cubic Co. A diffused ring results from very small clusters (less than a few nanometers), where most of the atoms are on surface sites and often deviate from the crystalline lattice of their corresponding bulk crystal. In this early stage, from 86 to 171 s when Li_2O crystals did not nucleate, the small clusters
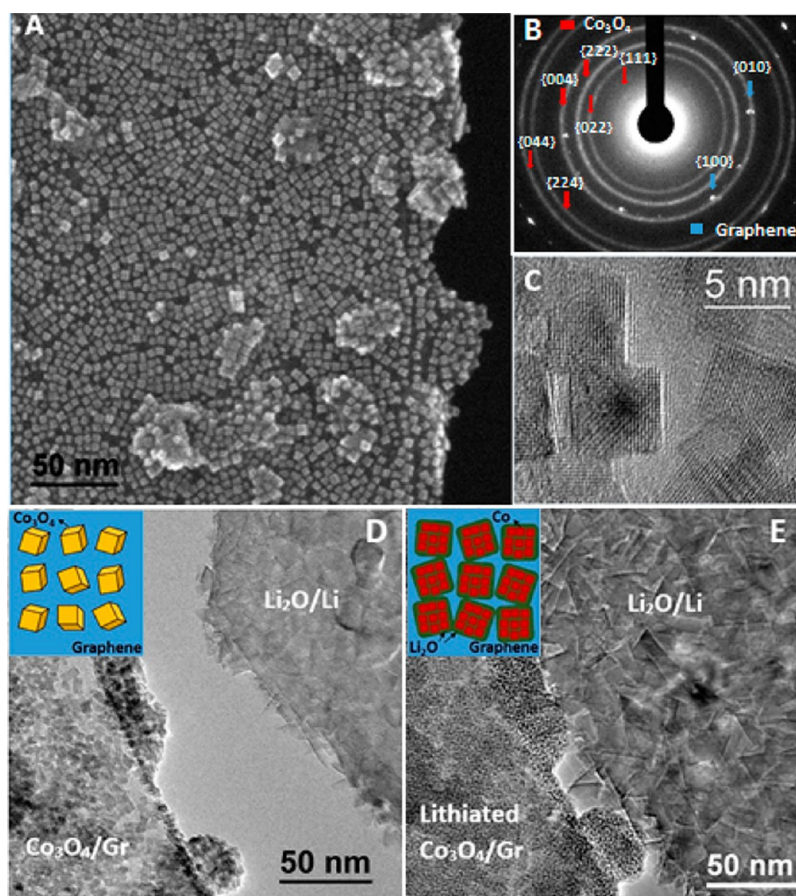
Figure 1. Co_3O_4 nanoparticles on few-lay graphene (Co_3O_4/graphene) and their lithiation by *in situ* TEM. (A) SEM image, (B) SAED, and (C) HREM image of graphene-supported Co_3O_4 nanocubes. (D) Co_3O_4/graphene and Li_2O/Li mounted on the tip of *in situ* TEM holder. (E) Chemical lithiation of Co_3O_4/graphene when they were brought into contact with Li_2O/Li. Insets in (D,E) illustrate the phase transformation.

formed should be partially reduced Co_3O_4 intercalated with Li^+ ions, called Co—O—Li clusters. As reaction time increases, the diffraction rings of Li_2O appeared at about 171 s and became stronger and stronger, implying that the Li_2O crystal grows larger and with higher crystalline quality. However, the diffused ring (corresponding to 0.20—0.21 nm) remains diffuse. The final Co-rich product of the reaction was identified as Co^0 (metallic) nanoparticles, as the charge state of Co could be readily determined by electron energy loss spectra (EELS) as shown in Supporting Information Figure 2, by which the reduction of pristine Co_3O_4 to Co was confirmed.

We employed nanobeam electron diffraction to further characterize the reaction products. In the nanobeam diffraction pattern (Supporting Information Figure 3), the diffused ring remains similar while the diffraction rings of Li_2O and graphene became clear and sharp. The ring remains diffused even in the nanobeam diffraction pattern, implying that the sizes of the Co^0 clusters are quite small even after the Co—Li—O clusters have been further reduced into Co clusters.

The electrochemical conversion reaction during Co_3O_4 lithiation was further studied by *in situ* high-resolution electron microscopy at atomic resolution to investigate the reaction pathway and mechanism down to atomic-scale spatial discrimination. Figure 2A shows HREM images of Co_3O_4 nanocubes on graphene which is a screenshot from Supporting Information movie 2. In the images, some large black dots (about 0.5 nm shown by a yellow arrowhead) with steady contrast, which does not change along with imaging defocus, are identified as Co-rich clusters. The contrast mainly originates from absorption and is thus sensitive to heavy elements (which is Co in this case), unlike the phase contrast which shows the lattice fringes in the HREM image. Figure 2A is used as the starting point in the time domain to monitor the progress of the reaction.

The three stages in the lithiation can be discerned from Supporting Information movie 2, with respect to current experimental settings. First, from 0 to 120 s, the nanocubes expanded about 14% two-dimensionally, as measured in the HREM images shown in Figure 2A—D, while its crystalline structure is maintained, as indicated by the {111} lattice fringes in the images. In the second stage (Figure 2D—F), the nanocube's crystalline lattice collapses and its 2D area expands about 25%. Nucleation of Co-rich clusters
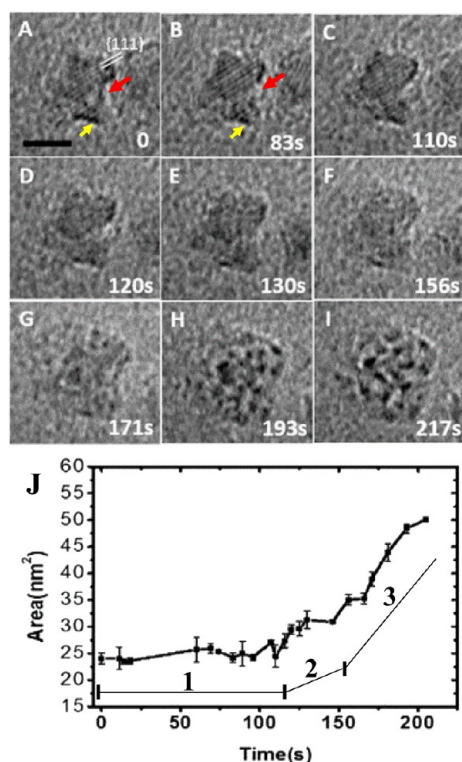
Figure 2. *In situ* HREM of lithiation of a Co_3O_4 nanocube on few-layer graphene. (A−I) Time-resolved HREM images of the lithiation process with time labeled and (J) plot of the projected area of the lithiated Co_3O_4 nanocube *vs* lithiation time. The scale bar is 5 nm.

can be observed throughout the whole nanocube. In the third stage (Figure 2G−I), the nanocube further expands almost 55% in its 2D area. Meanwhile, the Co-rich clusters grow and form a cluster network. The expansion of the nanocube is shown in Figure 2J, in which the three stages are labeled.

By considering additional information observed in diffraction (Supporting Information Figure 1) and EELS spectra (Supporting Information Figure 2), we propose the structural evolution in the conversion reaction of the Co_3O_4 as shown in Figure 3. In stage 1, the lithium ions are incorporated into the spinel lattice by insertion, forming an intercalated phase with a small volume expansion, such as $Li_xCo_3O_4$, as shown in Figure 3B.[15−17] With more and more lithium ions diffusing to react with Co_3O_4, the lattice finally collapses, leading to the formation of small Co−Li−O clusters (Figure 3C) in stage 2. As confirmed by diffraction (Supporting Information Figure 1), there exists a stage when Co−Li−O clusters can be identified but Li_2O crystals are not yet formed. In stage 3 (Figure 3D), small domains of Li_2O crystals nucleate and grow, accompanied by large volume expansion. The Co-rich clusters are further reduced to form neutral Co^0 clusters and are interconnected. It is worth noting that the formation of Li_2O introduces large volume expansion as Li_2O can intake more lithium ions (two lithium ions per oxygen). As early as stage 1, Co-rich clusters can be

formed on either surface or on an area with defects (as shown by the arrowheads in Figure 2A,B). It is on such a defective area that the Co-rich clusters preferentially nucleated and grew, as can be seen from the discontinuance of lattice fringes.

The products of the lithiation were confined to the graphene layers, which strongly suggests that the graphene layers served as an excellent support, even under large volume expansion. As measured from Figure 2, the total 2D area expansion is ∼120%, which is larger than the theoretical 3D volume expansion of the conversion reaction, which is around 100%. This implies that the product collapses onto and spreads out on the graphene layers after reaction. The Li_2O nanocrystals in the lithiated product have been further characterized by EELS and HREM. By using the absorption edge at 50.2 eV, which is a typical edge for Li_2O as labeled in Supporting Information Figure 4A, Li_2O nanocrystals are seen to be mostly distributed within the lithiated particles, as shown in Supporting Information Figure 4C−G. From the HREM image (Supporting Information Figure 5), the Li_2O crystal can be seen near Co nanoparticles. The Li_2O crystals likely provide a preferential substrate on which Li_2O can further grow in the battery run with liquid electrolyte. This may cause a very large irreversible capacity at the first cycle.

Delithiation (Deconversion Reaction) with Extraction of the Lithium Ion during the Charging Cycle. The deconversion reaction is generally energy unfavorable because the Li_2O is chemically more stable than other metal oxides (*e.g.*, Co_3O_4). An external potential has to be applied to initiate the deconversion reaction. When a positive potential (*e.g.*, 3 V) is applied on the Nanofactory holder, it is the process corresponding to delithiation and deconversion reaction. Using *in situ* TEM, we have observed different delithiation approaches and products which can be related to the different levels of potential to which the cell has been charged (refer to the half-cell setting where lithium metal is used as the anode and Co_3O_4 as the cathode). In our experimental settings, although the applied external potential can be controlled, the localized potential applied to a nanoscale area is influenced by other factors that cannot be controlled, such as the thickness of the effective solid electrolyte or localized conductivity. When a localized potential has not effectively been applied (possibly related to the fact that the cell was charged to <1 V), recrystallization of the graphene layers is observed in the delithiation, as shown in Supporting Information Figure 6A−D. In the diffraction patterns after about 968 s of delithiation, the diffused ring corresponding to Co clusters and rings of Li_2O nanocrystals can still be observed, implying that major Li_2O dissociation and oxidation of Co clusters have not yet occurred. At low potential, the extraction of the lithium ion occurs mostly from graphene layers, leading to recrystallization of the graphite. This is
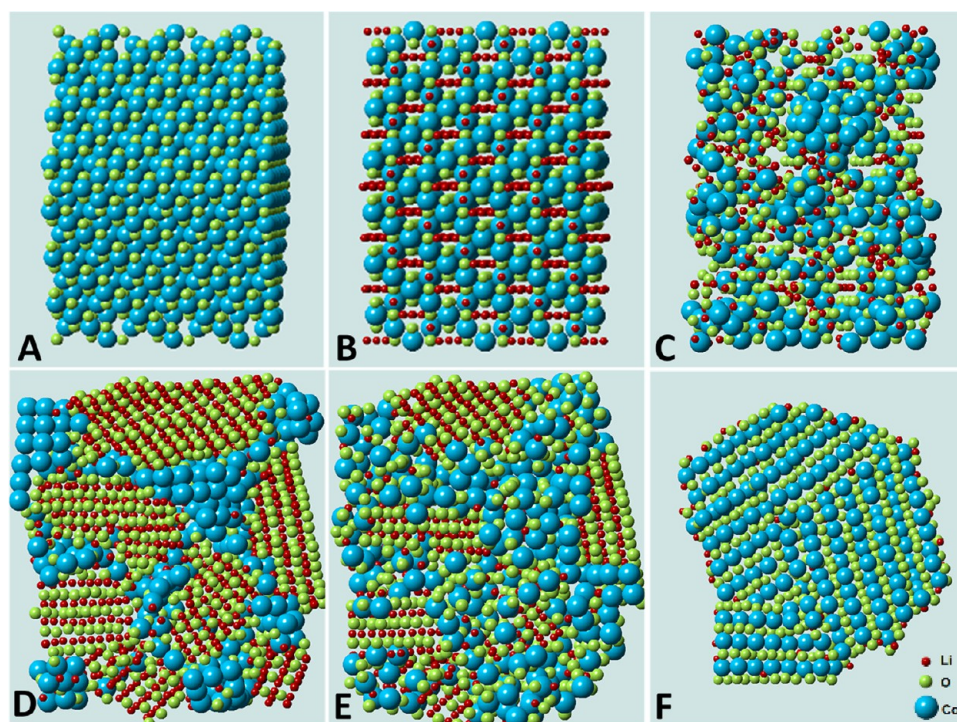
Figure 3. Schematic atomistic models of the lithiation/delithiation process of a single Co_3O_4 nanocube. Co, blue; O, green; Li, red. (A) Spinel Co_3O_4 before lithiation, (B) initial stage of Li-ion insertion with the formation of $Li_xCo_3O_4$, (C) formation of Co-rich Co−Li−O clusters with further intake of Li-ion, (D) formation of interconnected Co^0 clusters embedded in the Li_2O nanocrystals, (E) dissociation of the Co^0 clusters to form smaller clusters in the initial stage of delithiation, and (F) formation of CoO nanoparticles as the lithiation product by a deconversion reaction.

consistent with the fact that the electrochemical potential needed for the deconversion reaction to occur is higher than that of delithiation of graphite.

When a localized potential is effectively applied (possibly related to the fact that the cell is charged up to a normal range such as 2−3 V), a heterogeneous transformation, due to the deconversion reaction, can be observed. The Li_2O is dissociated along with the oxidation of the Co clusters, leading to the formation of nanocrystals with CoO cubic structure (NaCl-type face-centered cubic, *fcc*), as illustrated in Figure 3E,F. The phase transformation has been monitored by electron diffraction. The diffused ring (0.20−0.21 nm) shown in Supporting Information Figure 7A is replaced by the other diffused ring with *d*-spacing of 0.25−0.27 nm, as shown in Supporting Information Figure 7B. The diffused ring of 0.25−0.27 originates from nano- and polycrystals of Li_2O {111} lattice planes and CoO {111} lattice planes. In Supporting Information Figure 7C, when most of the diffraction from Li_2O has become extremely weak, the phase left can be identified as *fcc* CoO, instead of Co_3O_4, by using nanobeam diffraction (as shown in Supporting Information Figure 7D). It has been reported that the delithiation product is CoO.[16,18] The average size of the CoO is about 4 nm (Supporting Information Figure 8). Using *in situ* HREM imaging, we also observed another surprising phenomenon in the phase transformation from Co clusters to CoO nanocrystals along with dissociation of Li_2O and

electrochemical extraction of lithium ions. As shown in Supporting Information movie 3 and Figure 4A−D, the Co-rich clusters with high contrast in the images have been partially dissolved to react with active O^{2-} anions/radicals, which prompts the dissociation of Li_2O and formation of CoO nanocrystals. After delithiation for about 60−120 s, Co metal clusters (3−5 nm, Figure 4A) disintegrate into smaller particles (2−3 nm, Figure 4B,C) along with the decomposition of Li_2O. After delithiation for about 300 s, the Co-rich cluster grows larger to an average size of 2.4 nm, and they are now most likely CoO nanoparticles (Figure 4D). When lithium was taken out from the Co−Li_2O composites at the beginning of the delithiation, the Co and oxygen having no direct contact would have to diffuse together to form CoO. Here, the disintegration of large Co clusters into smaller ones will increase the effective surface of Co to react with oxygen and shorten the diffusion path to prompt the reaction. Such observation could serve as an indirect proof that Co metal can act as not only a reactant but also a catalyst in the deconversion reaction.

When a large localized potential is applied (possibly related to an overcharge in the cell), the heterogeneous transformation due to the deconversion reaction occurs instantly, leading to the formation of large-sized CoO crystals (as shown in Supporting Information movie 4). As shown in Supporting Information Figure 9A, the average size of the CoO nanoparticles formed
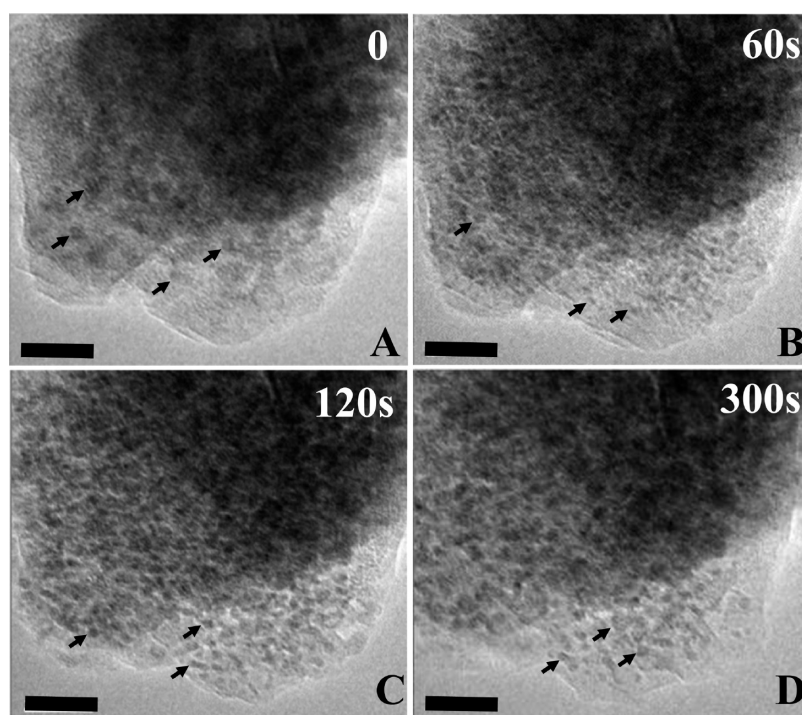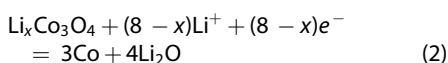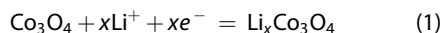
Figure 4. *In situ* HREM of the transformation from Co clusters to CoO nanoparticles on few-layer graphene in the delithiation. (A) Screen shot from Supporting Information movie 3 at 0 s showing Co clusters with an average size of ~3.2 nm. (B) After delithiation for 60 s, the Co-rich clusters became small with an average size of ~1.8 nm. (c) After delithiation for 120 s, the nanoparticles are CoO with an average size of 2.0 nm. (d) After delithiation for 300 s, the nanoparticles grew larger to have an average size of 2.4 nm. The scale bar is 10 nm. Some of the small nanoparticles are shown by arrowheads.
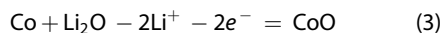
is ~20−30 nm, much larger than those formed when a moderate potential is applied. Their structure can be identified as *fcc* CoO, as shown in the inset of Supporting Information Figure 9B. Elementary mapping reveals that the large particles formed have an oxygen deficiency core (Supporting Information Figure 9C,D).

Structural evolution in the conversion and deconversion reactions with lithium ions, as revealed by *in situ* TEM, has many implications for understanding the intriguing phenomena observed in metal oxide electrodes. First, the effects of Co-rich clusters on the decomposition of thermodynamically stable Li_2O small crystals are directly observed and confirmed. In the deconversion reaction, these Co-rich clusters dissociate into smaller clusters, spreading out to react with O^{2-} anions, leading to the decomposition of Li_2O and formation of CoO. Second, the overpotential and voltage hysteresis can be better explained by looking at the reaction pathway revealed by the high-resolution *in situ* TEM.

Conversion:

$$Co_3O_4 + xLi^+ + xe^- = Li_xCo_3O_4 \qquad (1)$$

$$Li_xCo_3O_4 + (8-x)Li^+ + (8-x)e^- \\ = 3Co + 4Li_2O \qquad (2)$$

Deconversion:

$$Co + Li_2O - 2Li^+ - 2e^- = CoO \qquad (3)$$

Strictly speaking, the reaction is not reversible in the first cycle because the product of the deconversion

reaction (CoO) is different from the starting precursor (Co_3O_4) in the conversion reaction. This could be one of the causes for overpotential and voltage hysteresis. Third, several possibilities for explaining the extremely low initial Coulombic efficiency have been observed. For example, excess Li_2O can be easily formed on the substrates of the Li_2O crystal that is formed by the conversion reaction and not easily decomposed in the charge cycle. The efficient decomposition of Li_2O requires application of sufficient electrochemical potential and contact with Co clusters. However, along with the large volume expansion/contraction, there might be opportunities for the Co clusters to establish contact with some of the Li_2O layer and cause it to decompose, releasing the Li-ions and leading to additional reversible capacity in the following cycles. The reversible decomposition of excess Li_2O could surely lead to extra capacity, as observed in metal oxide run with conversion/deconversion reactions.

CONCLUSIONS

In summary, the structural evolution of Co_3O_4/graphene along with the electrochemical conversion/deconversion reactions has been studied at atomic resolution by *in situ* TEM to reveal the detailed reaction pathways and stages. In lithiation, a Li-inserted Co_3O_4 crystal and nanosized Co−Li−O clusters have been identified as medium products prior to the formation of Li_2O crystals in the conversion reaction. In delithiation,

the CoO nanoparticle has been identified as the product of the deconversion reaction. The electrochemical decomposition of Li$_2$O catalyzed by the nanosized Co clusters is an important process that determines the revisable capacity. Nanomaterials fully utilizing the catalytic property of Co clusters to decompose Li$_2$O may be feasible for developing high-power lithium-ion batteries that run on conversion reactions. Such *in situ* observations of the reaction pathway and conversion stages may provide necessary insights into further development of high-power lithium-air batteries based on reversible oxidation and reduction of Li$_2$O.

EXPERIMENTAL SECTION

Graphene-supported Co$_3$O$_4$ nanocubes were synthesized by a one-pot hydrothermal method. In a typical synthesis, a specific amount of cobalt(II) acetate tetrahydrate was dissolved in dimethylformamide (DMF) and water. Graphene prepared by sonication in organic solvent was then added into the above solution by stirring to form a suspension. Then the suspension was put into a Teflon-lined autoclave and sealed at room temperature. The stainless steel autoclave was then heated and kept at 120 °C for 2 h. After the autoclave was subsequently cooled to ambient temperature, the precipitate was collected by centrifugation, washed repeatedly with ethanol, and dried in an oven at 60 °C. The as-prepared samples were characterized by X-ray diffraction (Shimadzu XRD-6000, Cu Kα radiation, 1.5406 Å), selected area, and nanobeam electron diffraction in TEM (JEOL-2100F TEM and Hitachi HD2300 STEM) to be the Co$_3$O$_4$ phase. Also, the morphology of the nanocomposites was examined by the above TEM and STEM.

The open half-cell was constructed in an *in situ* electrical probing TEM holder (Nanofactory Instrument AB). This holder has a dual-probe design; that is, one Au rod is used as the sample holder with a small amount of Co$_3$O$_4$/graphene attached to its tip; on the other side, a STM tungsten probe driven by a piezo-motor capable of 3D positioning with a step size of 1 nm was used to mount the Li metal. The W probe tip was scratched by a Li metal strip and then affixed on the TEM holder inside an Ar-filled glovebox. With an airtight cover, the TEM holder was transferred to the TEM column with limited exposure to air (5 s), where a layer of lithium oxide was grown on the surface of Li metal and acted as a solid electrolyte for the nanocell Li-ion batteries. When the Au rod was negatively biased to −3 V, charging for Co$_3$O$_4$/graphene nanoparticles occurred, corresponding to the electrochemical lithiation of the nanoparticles. When a potential of +3 V was applied, a delithiation reaction of the nanoparticles occurred.

Conflict of Interest: The authors declare no competing financial interest.

Supporting Information Available: Nine supplementary figures and four supplementary movies are present as Supporting Information. This material is available free of charge *via* the Internet at http://pubs.acs.org.

REFERENCES AND NOTES

1. Idota, Y.; Kubota, T.; Matsufuji, A.; Maekawa, Y.; Miyasaka, T. Tin-Based Amorphous Oxide: A High-Capacity Lithium-Ion-Storage Material. *Science* **1997**, *276*, 1395–1397.
2. Poizot, P.; Laruelle, S.; Grugeon, S.; Dupont, L.; Tarascon, J. M. Nano-Sized Transition-Metal Oxides as Negative-Electrode Materials for Lithium-Ion Batteries. *Nature* **2000**, *407*, 496–499.
3. Cabana, J.; Monconduit, L.; Larcher, D.; Rosa Palacin, M. Beyond Intercalation-Based Li-Ion Batteries: The State of the Art and Challenges of Electrode Materials Reacting through Conversion Reactions. *Adv. Mater.* **2010**, *22*, E170–E192.
4. Li, H.; Balaya, P.; Maier, J. Li-Storage *via* Heterogeneous Reaction in Selected Binary Metal Fluorides and Oxides. *J. Electrochem. Soc.* **2004**, *151*, A1878–A1885.
5. Liao, P.; MacDonald, B. L.; Dunlap, R. A.; Dahn, J. R. Combinatorially Prepared LiF$_{(1-x)}$Fe$_{-x}$ Nanocomposites for Positive Electrode Materials in Li-Ion Batteries. *Chem. Mater.* **2008**, *20*, 454–461.
6. Zhou, Y. N.; Liu, W. Y.; Xue, M. Z.; Yu, L.; Wu, C. L.; Wu, X. J.; Fu, Z. W. LiF/Co Nanocomposite as a New Li Storage Material. *Electrochem. Solid-State Lett.* **2006**, *9*, A147–A150.
7. Zhou, Y.; Wu, C.; Zhang, H.; Wu, X.; Fu, Z. Electrochemical Reactivity of Co-Li$_2$S Nanocomposite for Lithium-Ion Batteries. *Electrochim. Acta* **2007**, *52*, 3130–3136.
8. Hu, Y.-Y.; Liu, Z.; Nam, K.-W.; Borkiewicz, O. J.; Cheng, J.; Hua, X.; Dunstan, M. T.; Yu, X.; Wiaderek, K. M.; Du, L.-S.; *et al.* Origin of Additional Capacities in Metal Oxide Lithium-Ion Battery Electrodes. *Nat. Mater.* **2013**, *12*, 1130–1136.
9. Huang, J. Y.; Zhong, L.; Wang, C. M.; Sullivan, J. P.; Xu, W.; Zhang, L. Q.; Mao, S. X.; Hudak, N. S.; Liu, X. H.; Subramanian, A.; *et al. In Situ* Observation of the Electrochemical Lithiation of a Single SnO$_2$ Nanowire Electrode. *Science* **2010**, *330*, 1515–1520.
10. Liu, X. H.; Wang, J. W.; Huang, S.; Fan, F.; Huang, X.; Liu, Y.; Krylyuk, S.; Yoo, J.; Dayeh, S. A.; Davydov, A. V.; *et al. In Situ* Atomic-Scale Imaging of Electrochemical Lithiation in Silicon. *Nat. Nanotechnol.* **2012**, *7*, 749–756.
11. Su, Q.; Xie, D.; Zhang, J.; Du, G.; Xu, B. *In Situ* Transmission Electron Microscopy Observation of the Conversion Mechanism of Fe$_2$O$_3$/Graphene Anode during Lithiation−Delithiation Processes. *ACS Nano* **2013**, *7*, 9115–9121.
12. Wang, F.; Yu, H.-C.; Chen, M.-H.; Wu, L.; Pereira, N.; Thornton, K.; Van der Ven, A.; Zhu, Y.; Amatucci, G. G.; Graetz, J. Tracking Lithium Transport and Electrochemical Reactions in Nanoparticles. *Nat. Commun.* **2012**, *3*, 1201.
13. Lin, F.; Nordlund, D.; Weng, T.-C.; Zhu, Y.; Ban, C.; Richards, R. M.; Xin, H. L. Phase Evolution for Conversion Reaction Electrodes in Lithium-Ion Batteries. *Nat. Commun.* **2014**, *5*, 3358.
14. Luo, L.; Wu, J.; Luo, J.; Huang, J.; Dravid, V. P. Dynamics of Electrochemical Lithiation/Delithiation of Graphene-Encapsulated Silicon Nanoparticles Studied by *In-Situ* TEM. *Sci. Rep.* **2014**, *4*, 3863.
15. Thackeray, M. M.; Baker, S. D.; Adendorff, K. T.; Goodenough, J. B. Lithium Inserion into CO$_3$O$_4$—A Preliminary Investigation. *Solid State Ionics* **1985**, *17*, 175–181.
16. Larcher, D.; Sudant, G.; Leriche, J. B.; Chabre, Y.; Tarascon, J. M. The Electrochemical Reduction of Co$_3$O$_4$ in a Lithium Cell. *J. Electrochem. Soc.* **2002**, *149*, A234–A241.
17. Shaju, K. M.; Jiao, F.; Debart, A.; Bruce, P. G. Mesoporous and Nanowire Co$_3$O$_4$ as Negative Electrodes for Rechargeable Lithium Batteries. *Phys. Chem. Chem. Phys.* **2007**, *9*, 1837–1842.
18. Fu, Z. W.; Wang, Y.; Zhang, Y.; Qin, Q. Z. Electrochemical Reaction of Nanocrystalline Co$_3$O$_4$ Thin Film with Lithium. *Solid State Ionics* **2004**, *170*, 105–109.